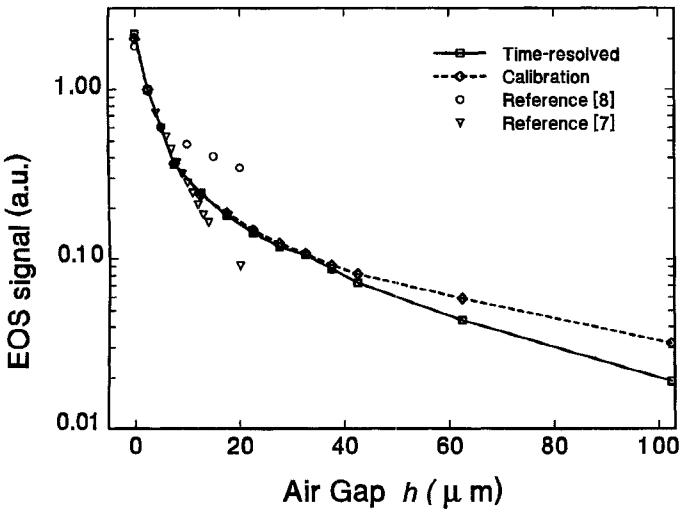

Fig. 4. EOS sensitivity as a function of air gap h. The solid and dashed lines connect the points shown by squares and diamonds, for time-resolved and calibration signals, respectively. The triangles and the circles are the data of [7] and [8], respectively.

IV. Summary

We have studied invasiveness and sensitivity of $LiTaO_3$ external probes for electrooptic sampling of millimeter-wave circuits and devices. Our measurements show two effects that contribute to distortion of the measured signals. The first is dispersion on the coplanar stripline caused by the presence of the $LiTaO_3$ superstrate. However, even once this dispersion is insignificant, pulse distortion is observed that we attribute to frequency-dependent signal reflection at the front probe facet. Both of these distortions can be reduced by using a noncontact arrangement with an air gap between the tip and the transmission line.

References

[1] J. A. Valdmanis, "Electro-optic measurement techniques for picosecond materials, devices, and integrated circuits," in *Measurement of High-Speed Signals in Solid State Devices,* R. B. Marcus, Ed. San Diego: Academic, 1990, pp. 136–219.

[2] A. Zeng, M. K. Jackson, M. Van Hove, and W. De Raedt, "On-wafer characterization of $In_{0.52}Al_{0.48}As/In_{0.53}Ga_{0.47}As$ modulation-doped field-effect transistor with 4.2 ps switching time and 3.2 ps delay," *Appl. Phys. Lett.,* pp. 262–263, 1995.

[3] M. Y. Frankel, J. F. Whitaker, and G. A. Mourou, "Optoelectronic transient characterization of ultrafast devices," *IEEE J. Quantum Electron.,* pp. 2313–2324, 1991.

[4] M. Y. Frankel, J. F. Whitaker, G. A. Mourou, and J. A. Valdmanis, "Experimental characterization of external electrooptic probes," *IEEE Microwave Guided Wave Lett.,* pp. 60–62, 1991.

[5] W. Mertin, C. Roths, F. Taenzler, and E. Kubalek, "Probe tip invasiveness at indirect electro-optic sampling of MMIC," in *'93 IEEE MTT-S Int. Microwave Symp. Dig.,* 1993, pp. 1351–1354.

[6] W. Von Wendorff, G. David, U. Dursum, and D. Jager, "Frequency domain characterization of a GaAs coplanar waveguide up to 40 GHz by electro-optic probing," in *Conf. Proc. LEOS '92,* 1992, pp. 119–121.

[7] T. Nagatsuma, T. Shibata, E. Sano, and A. Iwata, "Non-contact electro-optic sampling system in subpicosecond regime," in *IEEE Instrument. Measure. Tech. Conf. '90,* 1990, pp. 152–158.

[8] X. Wu, D. Conn, J. Song, and K. Nickerson, "Invasiveness of $LiTaO_3$ and GaAs probes in external E-O sampling," *J. Lightwave Technol.,* pp. 448–454, 1993.

Analysis of Microstrip Discontinuities Using the Spatial Network Method with Absorbing Boundary Conditions

Dragos Bica and Benjamin Beker

***Abstract*—In this paper it is shown that spatial network method (SNM) can be formally derived as a finite differencing scheme, which ensures that the necessary stability and convergence conditions are met. For the first time, Mur and Higdon second-order absorbing boundary conditions (ABC's) have been used in conjunction with SNM. It has been found that the Higdon second-order ABC's perform better than the Mur algorithm for guided wave problems with inhomogeneous substrates. Finally, it is shown that SNM can successfully be employed for the analysis of planar and three-dimensional (3-D) microstrip discontinuities in open or shielded environments.**

I. Introduction

During the past decade, the interest in microstrip discontinuities has substantially increased, as can be seen from the growing number of reported research activity on the subject [1]–[5], [12], and [13]. The driving factors behind this trend are increasing frequencies of operation and the continuing need for more accurate design methods for microwave integrated circuits (MIC's). Some microstrip discontinuities, such as steps and bends are due to the interconnects of various MIC's. Others, such as tuning stubs or resonant strips, are used to achieve specific functionality.

Several methods have already been employed for the study of microstrip discontinuities. Green's function based methods, such as the integral equation in spectral domain method [1] or the time domain method of lines [2], have been used to characterize planar discontinuities (open ends, stubs, gaps, steps in width) as well as full 3-D problems such as vias and air bridges [3]. Compared against experimental data, these methods offer very accurate numerical results. The aforementioned methods provide the frequency response of the discontinuity, taking into account the boundary conditions which are built into the Green's functions. However, for complex, nonplanar geometries and for inhomogeneous substrates, such methods are difficult to implement, and volumetric methods are often used instead.

Examples of volumetric methods are the finite difference time domain (FDTD) technique, transmission line matrix method (TLM), and spatial network method (SNM). All of them have been used in the study of microstrip discontinuities. The TLM method, in its frequency domain form, has been used to calculate the S-parameters of transmission line interconnects such as vias and air bridges [4]. The FDTD method has been applied to the study of step, open end, and gap microstrip discontinuities [5].

Time domain differential equation methods can easily accommodate closed boundary conditions associated with shielded structures, but they do not have the inherent ability to simulate the open boundary conditions. To overcome such limitations, several absorbing boundary conditions (ABC's) have been proposed [6]–[8], mostly for the FDTD method, and more recently for TLM [9]. The ABC's have low numerical reflectivity (<-25 dB) if used within appropriate limits, as shown in [8]. The errors introduced by the ABC's can be minimized

Manuscript received June 11, 1995; revised March 20, 1996. This work was supported in part by the US Army Research Office under Grant DAAL03-92-G-0275.

The authors are with the Department of Electrical and Computer Engineering, University of South Carolina, Columbia, SC 29208 USA.

Publisher Item Identifier S 0018-9480(96)04722-9.

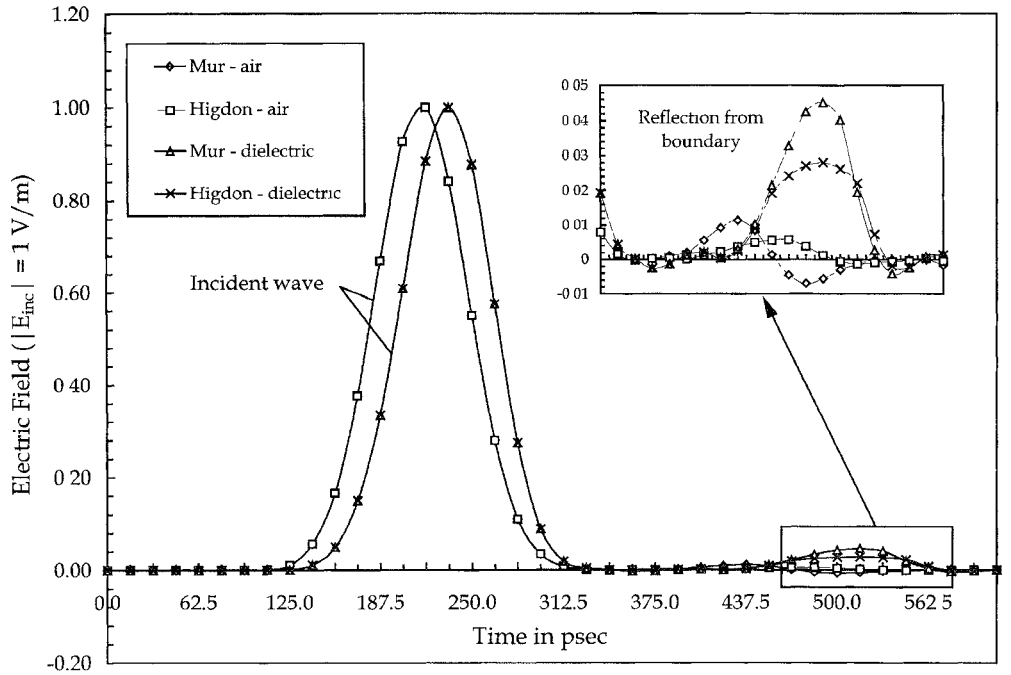

Fig 1 Reflections due to Mur and Higdon ABC's for shielded microstrip. Dimensions of the housing are 9 × 9 mm. Teflon substrate is 2.25 mm thick, and the strip is 3 75 mm wide

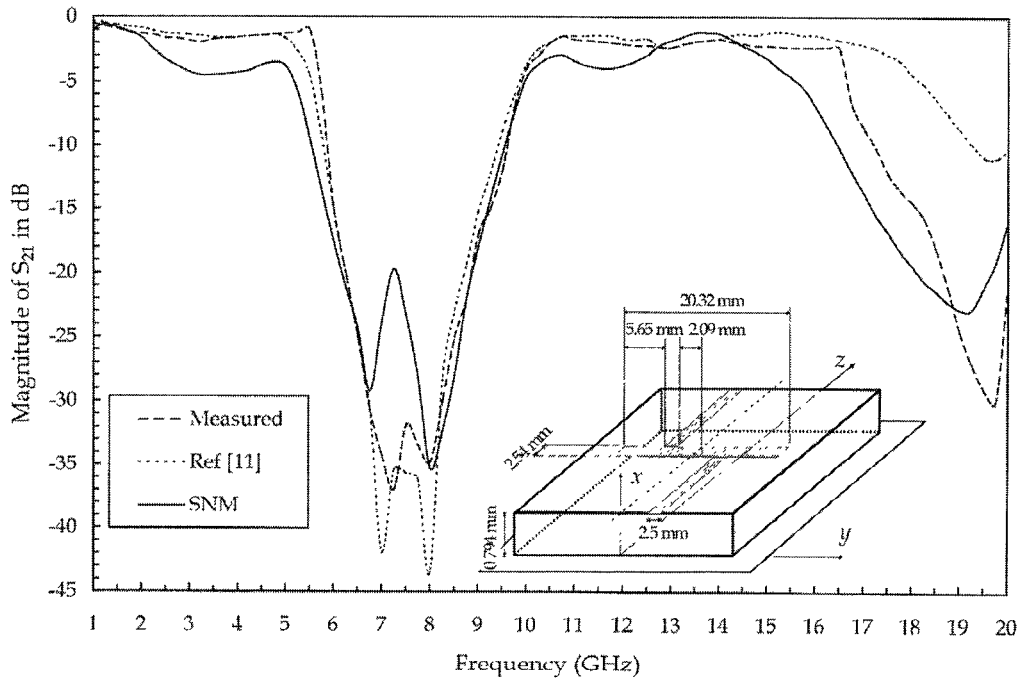

Fig. 2. $|S_{21}|$ of an open symmetric grounded stub.

using techniques such as the geometry rearrangement technique [10], which places the termination planes at equal distances away from the discontinuity.

The spatial network method (SNM) is derived from the differential form of Maxwell's equations using transmission line formalism and Bergeron's technique. It has been used in the study of waveguides, filters, bend discontinuities, and interconnects [11], [12]. However, numerical aspects of SNM, such as the convergence and stability of the algorithm, as well as a formulation of its finite differencing scheme, have not been formally addressed to date.

In this paper, a finite differencing scheme for SNM is given, and it shows that the algorithm has intrinsic stability, since the normalized algorithm velocity $c_0 \cdot \Delta t/\Delta x$ is predetermined by the transmission line equations. Under certain conditions, it is also shown that finite difference scheme employed in SNM has the same form as FDTD.

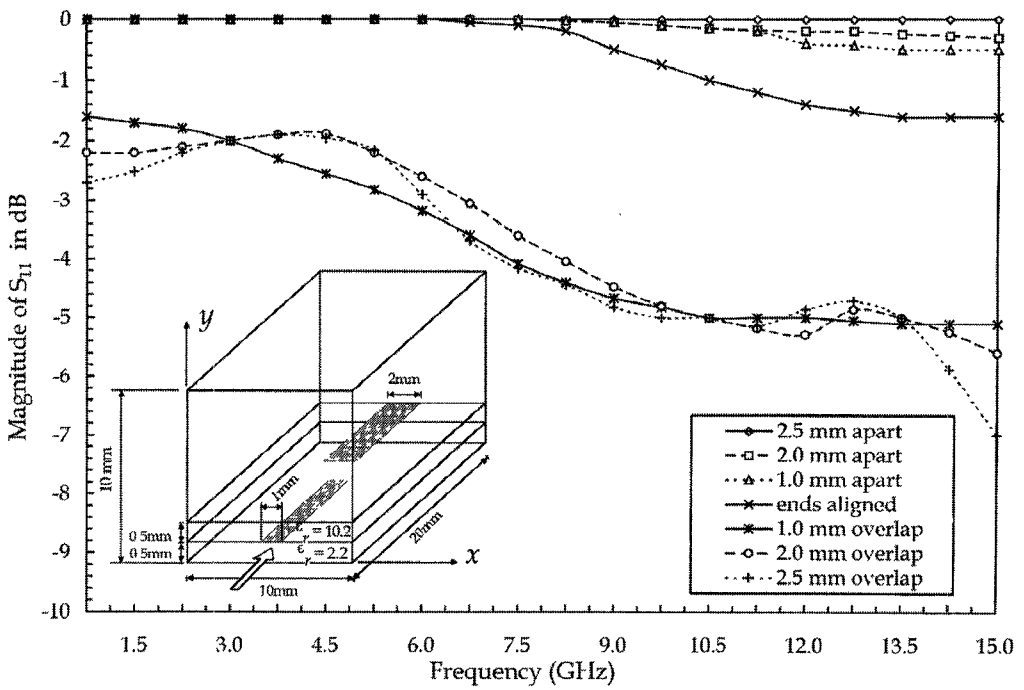

Fig. 3. $|S_{11}|$ of a 3-D two microstrip discontinuity as function of the overlap.

Until now, the use of second-order ABC's has not yet been attempted in SNM. In this paper, the second-order Higdon boundary operators are proposed for use in lattice truncation. For guided wave problems with inhomogeneous substrates the Higdon boundary conditions are found to keep numerical reflection levels to about -16 dB.

In order to validate the SNM/ABC's algorithm, the S-parameters of a symmetrical stub, were computed and compared against previously published and measured data. Finally, a multilayered structure, with two overlapping open end microstrips was also analyzed. This discontinuity may be used as a way of coupling transmission lines at very high frequencies. The S-parameters of this structure were computed as functions of the overlap dimensions and the frequency of excitation.

II. Summary of the Formulation

The basics of the SNM algorithm have been described extensively in [11] and [12]. For the electrical node associated with E_x (Fig. 3, [12]) the nodal equation can be written as

$$V_{ex}^{t+1}(i, j, k) = \frac{R_c \cdot (\Psi_1^m + \Psi_2^m + \Psi_3^m + \Psi_4^m) + Z_0 \cdot \Psi_c}{Z_0 + R_c \cdot [4 + Z_0 \cdot 4 \cdot G(i, j, k)]} \quad (1)$$

where

$$R_c = \frac{\Delta t \cdot c_0}{4 \cdot \varepsilon_0 \cdot \chi_e \cdot \Delta x},$$

$$G^{-1} = \frac{2 \cdot \Delta x}{\sigma = R}$$

and

$$Z_0 = \sqrt{\frac{\mu_0}{\varepsilon_0}}.$$

The terms Ψ_k^m, $k = 1, 2, 3, 4$ account for waves propagating toward the node on the four transmission lines attached to it. The term Ψ_c is associated with the flow of current through the capacitor placed at the E_x node joining the four transmission lines. Using normalizations $V_{mk} = V_{mk} \cdot \sqrt{\mu_o}$ and $V_{ek} = V_{ek} \cdot \sqrt{\varepsilon_o}$, where $k = x, y, z$, (1) can be expressed in a modified form, which makes a distinction between the electric and magnetic variables

$$V_{ex}^{t+1}(i, j, k) = \frac{\sum_k I_{mk}^t + \sum_{k=y,z} V_{mk}^t + g_{ce} \cdot V_{ex}^t(i, j, k) + I_{ecx}^t(i, j, k)}{4 + g_{ce} + g_c} \quad (2)$$

where

$$g_{ce} = \frac{Z_0}{R_c}$$

and

$$g_c = \frac{Z_0}{R}.$$

Subsequently the currents flowing through the ends of the transmission lines connected at the single E_x node are computed using $V_{ex}^{t+1}(i, j, k)$ and Ψ_k^m, $k = 1, 2, 3, 4$, as described in [12].

In order to illustrate SNM's conformity to finite differencing scheme, all currents in (2) must be expressed in terms of electric and magnetic voltages only. It can be shown that the current through the capacitor, using the recurrence expression obtained from $i = C \cdot (dV/dt)$, can be written

$$I_{eck}^t(i, j, k) = g_{cek} \cdot [V_{ek}^t(i, j, k) - 2 \cdot V_{ek}^{t-1}(i, j, k) + 2 \cdot V_{ek}^{t-2}(i, j, k) - \cdots + (-1)^t \cdot 2 \cdot V_{ek}^2(i, j, k) + (-1)^{t+1} \cdot 2 \cdot V_{ek}^1(i, j, k)]. \quad (3)$$

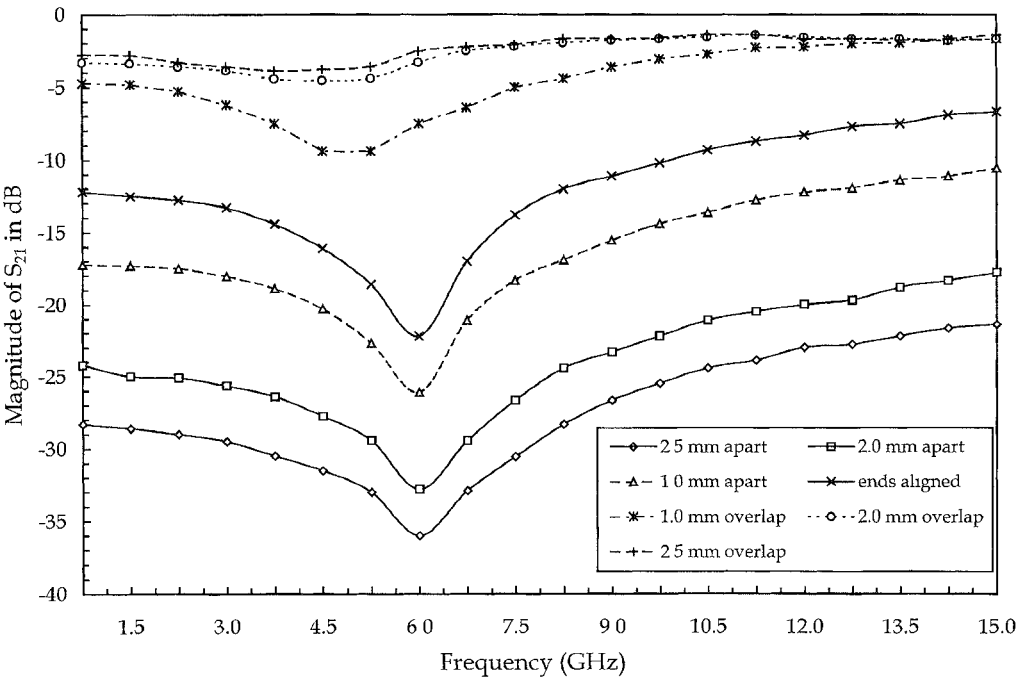

Fig. 4. $|S_{21}|$ of a 3-D two microstrip discontinuity as function of the overlap.

The use of (3) in (2) leads to the following finite difference form of SNM

$$E_x^{t+1}(i,j,k) = \frac{4}{4+g_c+g_{cex}} \cdot E_x^{t-1}(i,j,k) + \frac{g_{cex}}{4+g_c+g_{cex}} \cdot E_x^t(i,j,k) + \frac{2}{4+g_c+g_{cex}} \cdot [-H_z^t(i,j,k) + H_z^t(i,j+1,k) + H_y^t(i,j,k-1) - H_y^t(i,j,k)] + \frac{g_{cex}}{4+g_c+g_{cex}} \cdot [E_x^t(i,j,k) - 3 \cdot E_x^{t-1}(i,j,k) + 4 \cdot E_x^2(i,j,k) + \cdots + (-1)^{t+1} 2 \cdot E_x^1(i,j,k)]. \quad (4)$$

The above equation represents the finite difference scheme derived from a hyperbolic system of equations. In general, the conductance associated with the relative permittivity of the dielectric is defined as $g_{ce} = (\Delta x/\Delta t \cdot c_o) \cdot \varepsilon_r - 4$, and it is zero ($g_{ce} = 0$) if the dielectric is free space ($\varepsilon_r = 1$). In this case, (4) can be simplified as

$$E_x^{t+1}(i,j,k) = E_x^{t-1}(i,j,k) + \tfrac{1}{2} \cdot [-H_z^t(i,j,k) + H_z^t(i,j+1,k) + H_y^t(i,j,k-1) - H_y^t(i,j,k)] \quad (5)$$

which represents the FDTD discretization of Maxwell's curl equation for E_x with a Courant number of 0.5. In summary, the SNM algorithm and FDTD method belong to the same family of finite differencing schemes and they are identical for the particular case of free space dielectric.

To date, ABC's in SNM have only been implemented as matched loads terminating the outermost transmission lines at the lattice boundaries, but their behavior has not been analyzed in detail [12]. In this paper, the use of second-order Higdon absorbing boundary conditions for the SNM algorithm is proposed.

The second-order Higdon boundary conditions can be derived using the coefficient matrix proposed by Luebbers in [8]. With the help of the following notation: $b_i = (\alpha_i \cdot c \cdot \Delta t - \Delta x)/(\alpha \cdot c \cdot \Delta t + \Delta x)$, the second-order boundary conditions can be written as

$$E^{t+1}(0,j,k) = (b_1+b_2) \cdot E^t(0,j,k) - b_1 \cdot b_2 \cdot E^{t-1}(0,j,k) - (b_1+b_2) \cdot E^{t+1}(1,j,k) + (2-\xi_1-\xi_2-2 \cdot b_1 \cdot b_2) \cdot E^t(1,j,k) - [b_1 \cdot (1-\xi_2) + b_2 \cdot (1-\xi_1)] \cdot E^{t-1}(1,j,k) - b_1 \cdot b_2 \cdot E^{t+1}(2,j,k) + [b_1 \cdot (1-\xi_2) + b_2 \cdot (1-\xi_1)] \cdot E^t(2,j,k) - (1-\xi_1)(1-\xi_2) \cdot E^{t-1}(2,j,k). \quad (6)$$

These ABC's have been tested for a variety of problems ranging from plane wave scattering to partially loaded waveguides and totally open structures. The numerical reflections for the problems in this paper were as low as -23 dB for guided wave structures with uniform dielectric, but increased to -16 dB for transmission lines with inhomogeneous substrates.

III. Numerical Results

Both Mur and Higdon absorbing boundary conditions were tested in conjunction with the SNM algorithm. The emphasis of the study was placed on their behavior when applied to transmission line type structures. The Higdon ABC's performed better both for structures having uniform and nonuniform dielectrics. The overall results, displaying both the excitation and reflections from the truncated boundary at the open ends of a shielded uniform microstrip transmission line are shown in Fig. 1. The computational space in uniformly subdivided into a $l \times m \times n = 12 \times 12 \times 60$ lattice along the x-, y-, and z-directions, respectively, with $\Delta = 0.75$ mm. The E_x component is calculated midway along the z-axis at 1000 time steps ($\Delta t = 0.625$ ps). It can be seen that the Higdon absorbing boundary conditions have reflectivity of about -23 dB and -16 dB for uniform and nonuniform dielectric, respectively.

In all subsequent examples, the S-parameters were computed by taking FFT's of time domain wave forms. The simulations were

performed on a i486DX2-66 MHz PC requiring computing time of 2.5 ms per unit cell and time step. On a 90 MHz P5, the computing time was 0.9 ms per unit cell and time step.

To validate the combination of SNM with ABC's, the S-parameters were computed for a symmetric open stub-type structure, which is shown in the inset of Fig. 2. The S_{21} parameter of the double stub is shown in Fig. 2, from which it can be seen that the data obtained with SNM is similar to data published in [10]. Both results, as well as the measured data, predict resonant frequencies at about 8 and 19 GHz. The structure in Fig. 2 was discretized into a $l \times m \times n = 18 \times 61 \times 80$ lattice, with $\Delta = 0.4$ mm. The total simulation time was $t = 9000 \times \Delta t$, where $\Delta t = 0.444$ ps. The S_{21} parameters show a good agreement near the first resonance. The SNM also appears to predict the value of S_{21} at the second resonant frequency with better accuracy than FDTD, when compared to the measured data.

Finally, the use of SNM is demonstrated for the analysis of a 3-D microstrip discontinuity. The multilayered substrate, shown in the inset of Fig. 3, is placed inside a waveguide with shielded side walls and open ends. The inner ends of the two microstrips are allowed to overlap or be slightly apart. The structure is discretized such that $l \times m \times n = 21 \times 21 \times 41$, with $\Delta = 0.5$ mm. For $\Delta t = 0.83$ ps, the total simulation time was $t = 1600 \times \Delta t$. The computed S_{11} and S_{21} parameters are shown in Figs. 3 and 4, respectively. Notice that as the ends of the lines are brought closer together, the magnitude S_{11} decreases, while that S_{21} increases. At higher frequencies, on the other hand, when the lines are tightly coupled, the magnitude of S_{21} is higher than that of S_{11}.

IV. Conclusion

The SNM algorithm was presented as a formal statement of the finite difference numerical scheme for the solution of Maxwell's equations. It was shown that the second-order ABC's can be employed in SNM for lattice truncation when dealing with open region problems. SNM is utilized in the study of planar and multilayered microstrip discontinuities. For the multilayered structure, it is shown that the effects of the overlap dimensions are very influential on the S-parameters. It is found that the SNM simulations can be effectively performed on a PC, yielding results comparable in accuracy to those obtained on lager computing platforms.

References

[1] R. H. Jansen, "The spectral domain approach for microwave integrated circuits," *IEEE Trans. Microwave Theory Tech.*, vol. MTT-33, pp. 1043–1056, Oct. 1985.

[2] S. Nam, H. Ling, and T. Itoh, "Characterization of microstrip line and its discontinuities using the time-domain method of lines," *IEEE Trans. Microwave Theory Tech.*, vol. 37, no. 12, pp. 2051–2057, Dec. 1989.

[3] T. Becks and I. Wolff, "Analysis of 3-D metallization structures by a full wave spectral domain technique," *IEEE Trans. Microwave Theory Tech.*, vol. 40, no. 12, pp. 2219–2227, Dec. 1992.

[4] H. Jin and R. Vahldieck, "The frequency-domain transmission line matrix method—A new concept," *IEEE Trans. Microwave Theory Tech.*, vol. 40, no. 12, pp. 2207–2218, Dec. 1992.

[5] X. Zhang and K. K. Mei, "Time-domain finite difference approach to the calculation of the frequency-dependent characteristics of microstrip discontinuities," *IEEE Trans. Microwave Theory Tech.*, vol. 36, no. 12, pp. 1775–1787, Dec. 1988.

[6] G. Mur, "Absorbing boundary conditions for the finite-difference approximation of the time-domain electromagnetic-field equations," *IEEE Trans. Electromag. Compat.*, vol. EMC-23, no. 4, pp. 377–382, Nov. 1981.

[7] R. L. Higdon, "Numerical absorbing boundary conditions for the wave equation," *Math. Computation*, vol. 49, no. 179, pp. 61–91, July 1987.

[8] R. Luebbers, "FDTD for antennas and scattering," in *Short Course Notes from 10th Annual ACES Conf.*, Monterey, CA, 1994.

[9] C. Eswarappa and W. J. R. Hoefer, "One-way equation absorbing boundary conditions for 3-D TLM analysis of planar and quasiplanar structures," *IEEE Trans. Microwave Theory Tech.*, vol. 42, no. 9, pp. 1669–1677, Sept. 1994.

[10] X. P. Lin and K. Naishdaham, "A simple technique for minimization of ABC-induced error in the FDTD analysis of microstrip discontinuities," *IEEE Microwave Guided Wave Lett.*, vol. 4, no. 12, pp. 402–404, Dec. 1994.

[11] N. Yoshida and I. Fukai, "Transient analysis of a stripline having a corner in three-dimensional space," *IEEE Trans. Microwave Theory Tech.*, vol. MTT-32, no. 5, pp. 491–498, May 1984.

[12] T. Shibata, T. Hayashi, and T. Kimura, "Analysis of microstrip circuits using three dimensional full wave electromagnetic field analysis in time domain," *IEEE Trans. Microwave Theory Tech.*, vol. 36, no. 6, pp. 1029–1035, June 1988.

[13] L. Lapidus and G. H. Pinder, *Numerical Solutions of Partial Differential Equations in Science and Engineering.* New York: Wiley, 1982.

Input Impedance of a Coaxial Probe Located Inside a Rectangular Cavity: Theory and Experiment

M. S. Leong, L. W. Li, P. S. Kooi, T. S. Yeo, and S. L. Ho

Abstract— **In this work, theoretical and experizmental analyzes of input impedance of a coaxial probe located in a rectangular cavity are presented. The technique of dyadic Green function (DGF) and the method of moments (MM) are applied in the theoretical analysis. For the magnetic equivalent source with a $\hat{y}$-directed discontinuity, two alternative representations of magnetic DGF for a rectangular cavity are derived in this paper. Numerical input reactance and phase of the reflection coefficient at the base of the probe obtained using both the conventional form and the alternative representations of the DGF are compared with the experimental data collected. It is found that the computed results obtained utilizing alternative DGF's agree better with the measured data.**

I. Introduction

The probe radiation inside a rectangular waveguide or cavity is an interesting and old problem. Since Schwinger studied the single-post problem during World War II for small posts, there have been many new advances on this problem. First, Collin [1, 1st ed.], early in 1960; Al-Hakkak in 1969 [2]; and Williamson [3], [4] from 1972 to 1985, used an important assumption that the current could be effectively represented by a filamentary current located at the center of the probe. In 1983 and 1984, Leviatan [5], [6] and in 1987, Jarem [7] used the eight equivalent current filaments representation to replace the conducting post surface and modified the previous single post with a central current. In 1991, Jarem [8] and in 1992 Liang *et al.* [9] included the effects from the frill current due to the probe located

Manuscript received June 11, 1995; revised March 20, 1996.

The authors are with the Department of Electrical Engineering, Communications and Microwave Division, National University of Singapore, Singapore 119260.

Publisher Item Identifier S 0018-9480(96)04723-0.